THE JOURNAL OF PHYSICAL CHEMISTRY C

pubs.acs.org/JPCC Article

Paramagnetic Relaxation Enhancement in Hydrophilic Colloids Based on Gd(III) Complexes with Tetrathia- and Calix[4]arenes

Rustem Zairov,* Silvia Pizzanelli, Alexey P. Dovzhenko, Irek Nizameev, Anton Orekhov, Natalya Arkharova, Sergey N. Podyachev, Svetlana Sudakova, Asiya R. Mustafina, and Lucia Calucci

Cite This: https://dx.doi.org/10.1021/acs.jpcc.0c00312 Read Online

ACCESS | Metrics & More | Article Recommendations | Supporting Information

ABSTRACT: Hydrophilic colloids {PSS-[$Ln_2(TCAi)_2$] and PSS-[LnCA*i*], where *i* = 1, 2, or 3 and Ln = Gd or Tb} were prepared by precipitation of Gd(III) or Tb(III) complexes with tetrathiacalix[4]-arenes (TCA*i*) and calix[4]arenes bearing two 1,3-diketone groups (CA*i*) from dimethylformamide to an aqueous solution of poly(sodium 4-styrenesulfonate) (PSS). Dynamic light scattering and transmission electron microscopy demonstrated the formation of nanoparticles coated by the polymer. Luminescence decay measurements on Tb(III)-based colloids allowed hydration numbers of 2 and 4 per metal ion to be determined for PSS-[$Ln_2(TCAi)_2$] and PSS-[LnCA*i*] samples, respectively. Longitudinal and transverse water proton relaxivity values measured at 20.8 MHz were remarkably high for the PSS-[GdCA*i*] colloids but unexpectedly low for the PSS-[$Gd_2(TCAi)_2$] ones. ^{1}H fast field cycling nuclear magnetic resonance relaxometry was applied to shed light on the origin of the different relaxation enhancement in the investigated systems. Extremely slow exchange with the bulk of water molecules coordinated to Gd(III) and the scarce accessibility of Gd(III) sites to water were highlighted as the main causes of limited relaxivity.

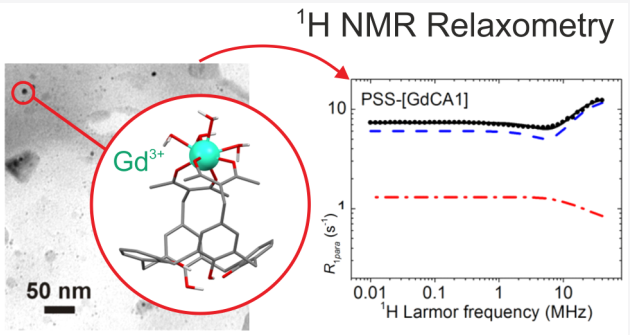

INTRODUCTION

Lanthanide-based nanoparticles have attracted a great deal of attention in recent years due to their applicability as contrast agents, which enables us to highlight cells or tissues by lanthanide-centered luminescence or lanthanide-induced enhancement of magnetic relaxation of water protons.[1−11] In particular, Gd(III)-based nanoparticles, showing large paramagnetic relaxation enhancement (PRE), can be a basis for improving contrast in magnetic resonance imaging (MRI) with respect to molecular Gd(III) complexes. In fact, embedding Gd(III) ions into nanostructures enhances water proton longitudinal relaxation by slowing the rotational motion of the Gd(III)−H_2O adduct. Moreover, the structure of the inner coordination sphere of the metal ion affects PRE through the number of coordinated water molecules (hydration number, *q*) and water exchange rate.[1,2,12−14] The accessibility of Gd(III) ions to water is also a fundamental parameter for PRE in Gd-containing nanoparticles. A greater enhancement is generally associated with Gd(III) centers localized on the nanoparticle surface compared to those in the interior and is favored by smaller particle sizes.[15,16]

Among the different strategies proposed for obtaining nanostructured Gd(III)-based systems showing pronounced PRE, solvent exchange or solvent-induced precipitation was highlighted as a facile route for converting water insoluble complexes of Gd(III) with calix[4]arene and calix[4]-resorcinarene ligands bearing tetra-1,3-diketone groups into polyelectrolyte-stabilized colloids, with a "hard" core constituted by aggregated complexes coated by a "soft" hydrophilic polymeric shell.[17−20] In these complexes, Gd(III) was chelated by two 1,3-diketonate groups, as determined by studying the Tb(III) counterparts in alkaline dimethylformamide (DMF) solutions.[21] This preparation route allows hydrophobic complexes, potentially suitable for biomedical applications because of the biocompatible polymeric coating, to be available in water.

In this work, this synthetic strategy was exploited to prepare for the first time "core-shell" colloids based on complexes of Gd(III) with two different classes of ligands, tetrathiacalix[4]-arenes and calix[4]arenes bearing bis-1,3-diketone groups (TCA*i* and CA*i*, where *i* = 1, 2, or 3 in Figure 1), using poly(sodium 4-styrenesulfonate) (PSS) as a coating polymer. These systems, hereafter termed PSS-[$Gd_2(TCAi)_2$] and PSS-[GdCA*i*], were characterized by dynamic light scattering

Received: January 13, 2020
Revised: January 20, 2020
Published: January 27, 2020

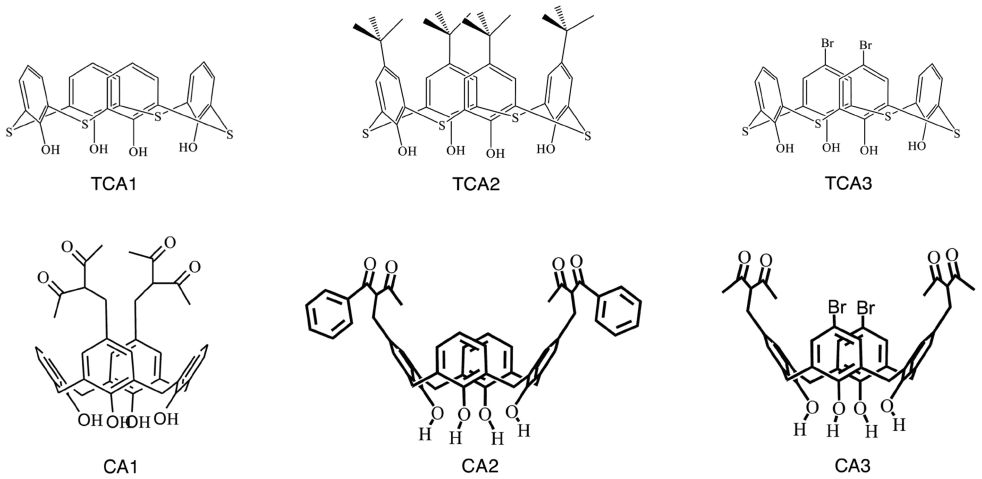

Figure 1. Structure of tetrathiacalix[4]arene (TCA*i*) and calix[4]arene (CA*i*) ligands (*i* = 1, 2, or 3).

(DLS), transmission electron microscopy (TEM), and cryo-TEM to investigate nanoparticle dimensions and colloid properties.

Different coordination modes were observed in a DMF solution for these two classes of ligands with Tb(III), as schematized in Figure 2. In the case of tetrathiacalix[4]arenes,

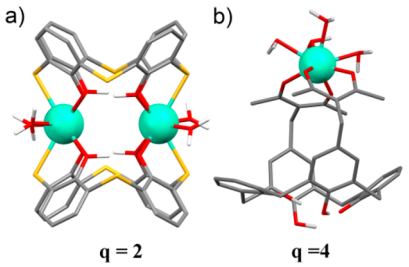

Figure 2. Schematic presentation of the coordination modes of Ln(III) ions in (a) [$Ln_2(TCAi)_2$] and (b) [LnCA*i*] complexes and their corresponding hydration numbers, *q*.

a sandwich coordination of two metal ions occurs through one S atom and the two adjacent O atoms belonging to two ligands, according to a 2:2 stoichiometry, as reported for TCA1.[22] On the other hand, all CA*i* ligands form 1:1 complexes using the two diketonate groups in the upper rim to chelate the metal,[23,24] in analogy to the tetra-1,3-diketone derivatives mentioned above. The coordination modes are expected to be associated with *q* values of 2 and 4 per metal ion, for the complexes with TCA*i* and CA*i* ligands, respectively (Figure 2).

These *q* values were here confirmed for the colloids prepared from isostructural Tb(III) complexes by luminescence measurements using the Horrocks equation.[25,26] However, relaxivity values, r_i, defined as the increase in relaxation rate R_i per millimolar Gd(III), with *i* = 1 and 2 for longitudinal and transverse relaxation, respectively, measured on Gd(III)-based colloids did not simply reflect the relative *q* values. In particular, PSS-[GdCA*i*] colloids showed a much higher relaxivity with respect to those of PSS-[$Gd_2(TCAi)_2$], and somewhat different values were determined within each class, indicating that several factors, at the molecular and nanoparticle level, play a role in relaxation enhancement.

To gain insight into the origin of the observed differences in relaxivity, ^{1}H fast field cycling nuclear magnetic resonance (FFC NMR) relaxometry[27,28] was applied. This technique, which measures the dependence of R_1 on the ^{1}H Larmor frequency over a broad range (0.01−35 MHz), coupled with PRE theory, is a powerful tool for characterizing Gd(III)-based contrast agents.[29] Notwithstanding the complexity of our systems, this method allowed precious indications to be obtained about the main parameters affecting the relaxivity properties of our colloids.

MATERIALS AND METHODS

Materials. PSS ($M_{Waverage}$ = 70000) (Acros Organics) and sodium chloride (Sigma-Aldrich) were used as received without further purification. DMF (Acros Organics) was twice distilled over P_2O_5. Gadolinium nitrate, $Gd(NO_3)_3 \cdot 6H_2O$ (99.9%), purchased from Sigma-Aldrich, and terbium nitrate, $Tb(NO_3)_3 \cdot 5H_2O$ (99.9%), purchased from Alfa Aesar, were used as received. Triethylamine, TEA (Acros Organics), and xylenol orange (Sigma-Aldrich) were used as received. CA*i*[23,24] and TCA*i*[30,31] ligands were synthesized as described in the literature. Ultrapure water (Milli-Q; 18.2 MΩ cm at 25 °C) was used in the colloid preparation.

Preparation of PSS-Stabilized Colloids. The samples were prepared according to the procedure reported in refs 18 and 19. Complexes of Ln(III) with TCA*i* and CA*i* ligands (*i* = 1, 2, or 3) were prepared by adding a DMF solution of $Gd(NO_3)_3 \cdot 6H_2O$ or $Tb(NO_3)_3 \cdot 5H_2O$ to a DMF solution containing the ligand and 4 equiv of TEA; the resulting concentration of both Ln and ligand was 4.5 mM. Colloids were obtained via precipitation of the water insoluble Ln(III) complexes from the DMF solution (1 mL) to a water solution of PSS (1 g/L, 5 mL, pH 6.0) containing NaCl (0.5 M). The DMF solution was added dropwise to the intensively stirred (2200 rpm) aqueous solution using a syringe pump. The obtained colloids, with a nominal Ln concentration of 0.75 mM, were sonicated for 30 min at 20 ± 2 °C and then centrifuged (10000 rpm, 15 min) to remove PSS excess; the supernatant was discarded, and the precipitate redispersed in water and sonicated. The procedure, including centrifugation, withdrawal of supernatant, redispersion, and sonication, was repeated.

Dynamic Light Scattering. DLS measurements were performed using a Malvern Mastersize 2000 particle analyzer operating with a He−Ne laser (633 nm) and emitting vertically polarized light as a light source. The effective hydrodynamic

https://dx.doi.org/10.1021/acs.jpcc.0c00312
J. Phys. Chem. C XXXX, XXX, XXX−XXX

radius (r_h) was calculated from the first cumulant using the Stokes–Einstein relation $D = k_B T/6\pi\eta r_h$, where D is the diffusion coefficient, k_B is the Boltzmann constant, T is the absolute temperature, and η is the viscosity. The diffusion coefficient was measured at least three times for each sample. The average error in these experiments is approximately 4%. Samples were prepared in deionized water, sonicated for 30 min, and equilibrated at 25.0 ± 0.1 °C before measurements.

Transmission Electron Microscopy. TEM images were obtained with a Libra 120 instrument (Carl Zeiss). Samples were sonicated in water for 30 min and then dispersed on 200 mesh copper grids with continuous Formvar support films. Images were acquired at an accelerating voltage of 100 kV.

Cryo-TEM. Cryo-TEM specimens were studied via bright field (BF) TEM in a Titan Krios 60–300 TEM/STEM instrument (FEI) equipped with a spherical aberration (Cs) corrector (image corrector), a direct detection camera Falcon II (FEI), and Volta phase plates.

Luminescence Spectroscopy. Luminescence spectra and lifetime measurements in the ultraviolet–visible (UV–vis) range were recorded using a Hitachi F-7100 spectrometer. A continuous-wave xenon lamp was used as the excitation source for steady state measurements, coupled to a double-grating monochromator for wavelength selection. Time-resolved photoluminescence emission was obtained in multichannel scaling (MCS) mode, exciting the sample by a microsecond xenon flashlamp with a pulse duration of 1–2 μs and a repetition frequency of 10 Hz.

Inductively Coupled Plasma Optical Emission Spectroscopy. Inductively coupled plasma optical emission spectroscopy (ICP-OES) measurements were performed using a PerkinElmer Optima 8000 instrument after treating the samples with 65% HNO_3 and 20% H_2O_2 and digesting them in a Milestone Start D microwave apparatus. Each measurement was performed twice.

^{1}H NMR Relaxometry Measurements. ^{1}H longitudinal (T_1) and transverse (T_2) relaxation times of water protons in PSS-[Gd_2(TCAi)$_2$] and PSS-[GdCAi] colloids, where i = 1, 2, or 3, were measured at 20.8 MHz using a spectrometer constituted by a Niumag permanent magnet interfaced with a Stelar PC NMR console (Stelar srl, Mede, Italy). The Inversion Recovery and Carr–Purcell–Meiboom–Gill pulse sequences were used to measure T_1 and T_2, respectively. Experiments were performed at 25 °C at different gadolinium concentrations, [Gd], obtained by dilution of each original sample, whose concentration was determined by ICP-OES. The temperature was controlled within ±0.5 °C with a Stelar VTC90 variable-temperature controller. Relaxivity values, r_i, where i = 1 or 2, were determined by fitting the trends of R_i versus [Gd] to the equation[12]

$$R_i = R_{i,0} + r_i[\mathrm{Gd}] \quad (1)$$

where $R_{i,0}$ is the diamagnetic contribution to the relaxation rate.

^{1}H T_1 values were measured at 25 °C in the 0.01–35 MHz Larmor frequency range using a SpinMaster FFC-2000 FFC NMR relaxometer (Stelar srl). T_1 measurements were performed using the prepolarized and non-prepolarized pulse sequences below and above 12 MHz, respectively. The polarizing and detection frequencies were 25.0 and 21.5 MHz, respectively. The switching time was 3 ms, and the 90° pulse duration 9.8 μs. A single scan was acquired. All of the other experimental parameters were optimized for each measurement. All of the ^{1}H magnetization curves versus time were monoexponential within experimental error, and the errors on R_1 were always <1%. The temperature was controlled within ±0.1 °C with a Stelar VTC90 variable-temperature controller.

Theoretical Basis. Gd(III) ions may induce PRE of water protons by inner sphere (IS) and outer sphere (OS) mechanisms.[12,32] The longitudinal relaxation rate arising from Gd(III), $R_{1,para}$ (=$R_1 - R_{1,0}$), is the sum of the IS and OS relaxation rates:

$$R_{1,para} = R_1^{IS} + R_1^{OS} \quad (2)$$

The IS mechanism involves the fluctuation of the dipolar interaction between the proton spin of water molecules bound to Gd(III) ions and the electron spin on the metal ($S = {}^7/_2$). The contribution to the relaxation rate from this mechanism, R_1^{IS}, depends on the concentration of Gd(III) ions, C_M; the hydration number, q; the mean residence time of the water molecules in the inner sphere, τ_m; the distance between Gd and water protons, r_{GdH}; the rotational correlation time of the Gd(III)–H vector, τ_R; and the relaxation times of the electronic spin, T_{ie}, where i = 1 or 2. According to the PRE theory based on the Solomon–Bloembergen–Morgan equations,[33,34] R_1^{IS} is given by

$$R_1^{IS} = \frac{qC_M}{1000 \times 55.55}\frac{1}{T_{1m} + \tau_m} \quad (3)$$

where C_M is expressed in millimolar, 55.55 is the molar concentration of water, and T_{1m} is the longitudinal relaxation time of the IS water protons. T_{1m} can be expressed as

$$\frac{1}{T_{1m}} = \frac{2}{15}\left(\frac{\mu_0}{4\pi}\right)^2 \frac{\gamma_H^2 g^2 \mu_B^2 S(S+1)}{r_{GdH}^6}\left(\frac{3\tau_{d1}}{1+\omega_H^2\tau_{d1}^2} + \frac{7\tau_{d2}}{1+\omega_S^2\tau_{d2}^2}\right) \quad (4)$$

where γ_H is the gyromagnetic ratio of the proton, g is the Landé factor, μ_B is the Bohr magneton, μ_0 is the vacuum permeability, and ω_H and ω_S are the proton and electron resonance frequencies ($\omega_S \cong 658\omega_H$), respectively. Rotational motion, relaxation of the unpaired electrons, and water exchange concur to determine the correlation times τ_{di} (where i = 1 or 2) according to the expression

$$\frac{1}{\tau_{di}} = \frac{1}{\tau_R} + \frac{1}{T_{ie}} + \frac{1}{\tau_m} \quad (5)$$

The electronic relaxation times, T_{ie}, can be written as[35]

$$\frac{1}{T_{1e}} = \frac{1}{25}\Delta^2\tau_v[4S(S+1) - 3]\left(\frac{1}{1+\omega_S^2\tau_v^2} + \frac{4}{1+4\omega_S^2\tau_v^2}\right) \quad (6)$$

$$\frac{1}{T_{2e}} = \frac{1}{50}\Delta^2\tau_v[4S(S+1) - 3]\left(\frac{5}{1+\omega_S^2\tau_v^2} + \frac{2}{1+4\omega_S^2\tau_v^2}\right) \quad (7)$$

https://dx.doi.org/10.1021/acs.jpcc.0c00312
J. Phys. Chem. C XXXX, XXX, XXX–XXX

where Δ^2 represents the mean square zero-field splitting (ZFS) of Gd(III) and τ_v is the correlation time associated with the modulation of the ZFS interaction.

The OS relaxation enhancement is due to the modulation of the dipolar interaction between water proton spins and the Gd electronic spin by the diffusion of water. The resulting relaxation rate, R_1^{OS}, depends on the distance of closest approach between water and Gd(III) ions, a_{GdH}, and on the relative diffusion constant of water and the paramagnetic center, D_{GdH}, according to the expression

$$R_1^{OS} = \frac{32\pi}{405}\left(\frac{\mu_0}{4\pi}\right)^2 \frac{\gamma_H^2 g^2 \mu_B^2 S(S+1)N_A}{a_{GdH} D_{GdH}} C_M[3J(\omega_H) + 7J(\omega_S)] \quad (8)$$

where N_A is Avogadro's number and the other parameters have the same meaning as in eqs 3 and 4. On the basis of the Huang and Freed theory,[36,37] spectral densities $J(\omega_H)$ and $J(\omega_S)$ can be expressed as

$$J(z_i) = Re\left(\frac{1 + \frac{z_i^{1/2}}{4}}{1 + z_i^{1/2} + \frac{4z_i}{9} + \frac{z_i^{3/2}}{4}}\right) \quad (9)$$

with

$$z_H = i\omega_H \tau_{GdH} + \frac{\tau_{GdH}}{T_{1e}} \quad (10)$$

and

$$z_S = i\omega_S \tau_{GdH} + \frac{\tau_{GdH}}{T_{2e}} \quad (11)$$

where the translational diffusion correlation time $\tau_{GdH} = a_{GdH}^2/D_{GdH}$.

RESULTS AND DISCUSSION

Preparation and Characterization of PSS-[Ln_2(TCA*i*)$_2$] and PSS-[LnCA*i*] Colloids. Complexes of Gd(III) or Tb(III) with TCA*i* and CA*i* ligands (Figure 1) were prepared in DMF by mixing Ln(III) ions and ligands in a 1:1 proportion. The 2:2 stoichiometry was established for the Tb(III) complexes with TCA1 from different physicochemical measurements in a previous work.[22] UV−vis spectra recorded in this work (Figure S1) indicate similarity in the spectral changes for all TCA*i*'s upon formation of the complex with Tb(III) in the DMF solution basified by TEA. Notably, no detectable deviations in the spectral data were revealed for Tb(III) and Gd(III) ions under the same concentration conditions. Job plots for TCA2 and TCA3 (Figure S1) point to the same stoichiometry and binding mode via O and S atoms as for the previously published [Tb_2(TCA1)$_2$] system (Figure 2), leaving the upper-rim substituents of insignificant impact. Thus, the 2:2 stoichiometry can be safely assumed also for the complexes with TCA2 and TCA3. The 1:1 stoichiometry of the [LnCA*i*] complexes was determined in previous studies for all CA*i* ligands,[22,24] with coordination to the Ln(III) ion through two diketonate groups (Figure 2).

PSS-stabilized nanoparticles were prepared via precipitation of water insoluble [Ln_2(TCA*i*)$_2$] and [LnCA*i*] complexes in an aqueous solution of PSS.[17,19] The colloids were washed from impurities and reagent excess through phase separation and redispersion cycles.

Colloidal properties of the PSS-[Tb_2(TCA*i*)$_2$] and PSS-[TbCA*i*] systems were investigated by different methods. DLS measurements showed an average size of the hydrated colloids of 80−136 nm and a rather low polydispersity index (Table 1),

Table 1. Hydrodynamic Diameters (d_h), Polydispersity Indices (PDI), and Electrokinetic Potentials (ζ) of PSS-[Tb_2(TCA*i*)$_2$] and PSS-[TbCA*i*] Colloids

	d_h (nm)[a]	PDI	ζ (mV)
PSS-[Tb_2(TCA1)$_2$]	109.3 ± 1.3	0.280 ± 0.031	−53.7 ± 2.2
PSS-[Tb_2(TCA2)$_2$]	82.3 ± 0.9	0.131 ± 0.005	−61.6 ± 4.9
PSS-[Tb_2(TCA3)$_2$]	80.9 ± 1.0	0.189 ± 0.027	−60.7 ± 0.6
PSS-[TbCA1]	124.6 ± 0.5	0.195 ± 0.006	−56.5 ± 2.7
PSS-[TbCA2]	101.9 ± 2.0	0.185 ± 0.025	−46.1 ± 1.8
PSS-[TbCA3]	135.6 ± 1.2	0.226 ± 0.017	−48.2 ± 3.9

[a] d_h values are obtained from the volume distribution.

indicating a narrow size distribution. The negative electrokinetic potential values (Table 1) confirm the "core-shell" morphology of the colloids, where the negatively charged PSS constitutes the exterior layer. Cryo-TEM allowed single spherical particles characterized by average diameters of 20−40 nm to be revealed for PSS-[Tb_2(TCA2)$_2$] (Figure S2), while TEM images of dried PSS-[Tb_2(TCA*i*)$_2$] colloids (Figure 3) indicated average size values of the nanoparticles ranging from 15 to 70 nm. For PSS-[TbCA*i*] colloids, TEM images (Figure 4) showed nanoparticle sizes between 2 and 12 nm. These dimensions can be explained by the presence of both single hard cores and their aggregates in the dried colloids, with a stronger tendency to aggregate exhibited by PSS-[Tb_2(TCA*i*)$_2$] samples compared to PSS-[TbCA*i*] ones. The greater average size obtained by DLS indicates that the PSS-coated colloids diffuse assembled in water.

In view of the investigation of relaxivity properties, the Gd concentration ($C_{M,ICP}$) was determined for PSS-[Gd_2(TCA*i*)$_2$] and PSS-[GdCA*i*] colloids by ICP-OES analysis. For the PSS-[Gd_2(TCA*i*)$_2$] samples, the $C_{M,ICP}$ values were between 0.62 and 0.68 mM, quite close to the nominal one ($C_{M,NOM}$ = 0.75 mM), whereas they ranged between 0.15 and 0.29 mM for the PSS-[GdCA*i*] colloids. ICP-OES and ^{1}H FFC NMR measurements were performed on supernatants of PSS-[Gd_2(TCA2)$_2$] and PSS-[GdCA1], taken as representative examples of colloids of thiacalix[4]arene and calix[4]arene complexes, to shed light on the fate of Gd(III) ions during the colloid preparation. An analogous investigation was performed for Tb(III) ions on the supernatants of the corresponding PSS-[Tb_2(TCA2)$_2$] and PSS-[TbCA1] colloids by spectrophotometric analysis using xylenol orange as an indicator.[38] The obtained results (see section S3 of Supporting Information) strongly indicate that in the precipitation step Ln(III) ions are released in water in the case of [LnCA*i*] complexes, but not in that of [Ln_2(TCA*i*)$_2$] complexes. Minor Ln(III) losses were found for all samples during the second washing.

Determination of the Hydration Number, *q*, by Luminescence Measurements. The coordination modes of the lanthanide complexes with ligands TCA*i* and CA*i* represented in Figure 2 point to a different hydration number *q* in the first coordination sphere of the corresponding Ln(III) complexes. This conjecture was verified for PSS-[Tb_2(TCA2)$_2$] and PSS-[TbCA1], chosen as being representative of the two complex classes, by the analysis of the

https://dx.doi.org/10.1021/acs.jpcc.0c00312
J. Phys. Chem. C XXXX, XXX, XXX−XXX

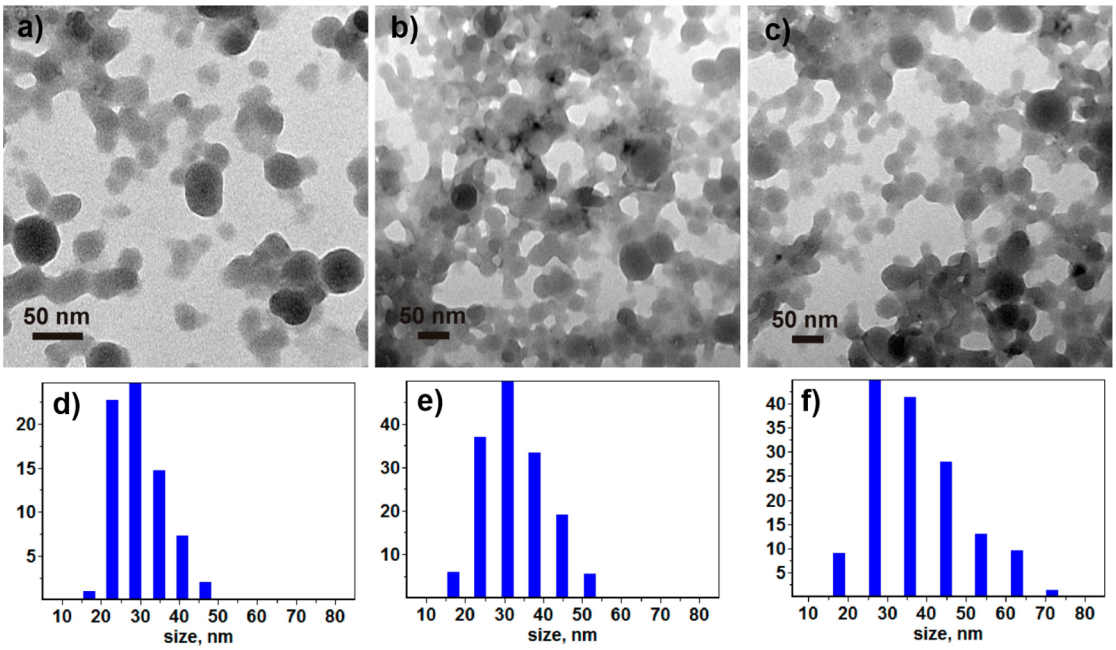

Figure 3. TEM images of (a) PSS-[$Tb_2(TCA1)_2$], (b) PSS-[$Tb_2(TCA2)_2$], and (c) PSS-[$Tb_2(TCA3)_2$]. (d–f) Corresponding nanoparticle size distribution diagrams.

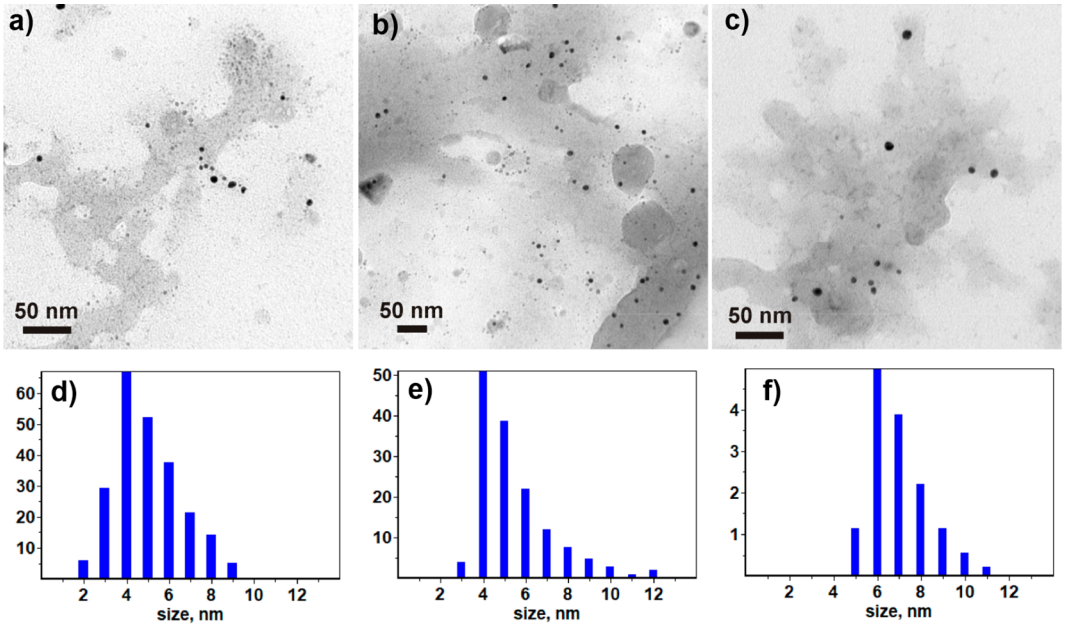

Figure 4. TEM images of (a) PSS-[TbCA1], (b) PSS-[TbCA2], and (c) PSS-[TbCA3]. (d–f) Corresponding nanoparticle size distribution diagrams.

emission lifetimes of Tb(III) complexes in H_2O (τ_{H_2O}) and D_2O (τ_{D_2O}) with the use of the Horrocks equation:[25,26]

$$q = A_{Tb}\left(\frac{1}{\tau_{H_2O}} - \frac{1}{\tau_{D_2O}}\right) \quad (12)$$

where A_{Tb} is a specific constant, defined empirically for Ln(III) chelates with known q values. A longer lifetime is indeed expected in D_2O because the deactivation by coordinated H_2O molecules via energy transfer to the O–H stretching vibration is not present. Fortunately, the investigated colloids exhibit efficient Tb(III)-centered luminescence, which is the prerequisite for the evaluation of q with an uncertainty of ±0.5.[19]

The steady state luminescence spectra of the representative PSS-[$Tb_2(TCA2)_2$] and PSS-[TbCA1] colloids (Figure 5) are characterized by four bands peculiar to Tb(III)-centered luminescence arising from $^5D_4 \rightarrow {}^7F_6$ (489 nm), $^5D_4 \rightarrow {}^7F_5$ (543 nm), $^5D_4 \rightarrow {}^7F_4$ (582 nm), and $^5D_4 \rightarrow {}^7F_3$ (620 nm) transitions. The intensity ratio of the bands at 543 and 489 nm (A_{543}/A_{489}) is sensitive to the ligand environment of Tb(III) ions. The different intensity ratios in the spectra of PSS-[$Tb_2(TCA2)_2$] ($A_{543}/A_{489} \cong 1.7$) and PSS-[TbCA1] ($A_{543}/$

https://dx.doi.org/10.1021/acs.jpcc.0c00312
J. Phys. Chem. C XXXX, XXX, XXX–XXX

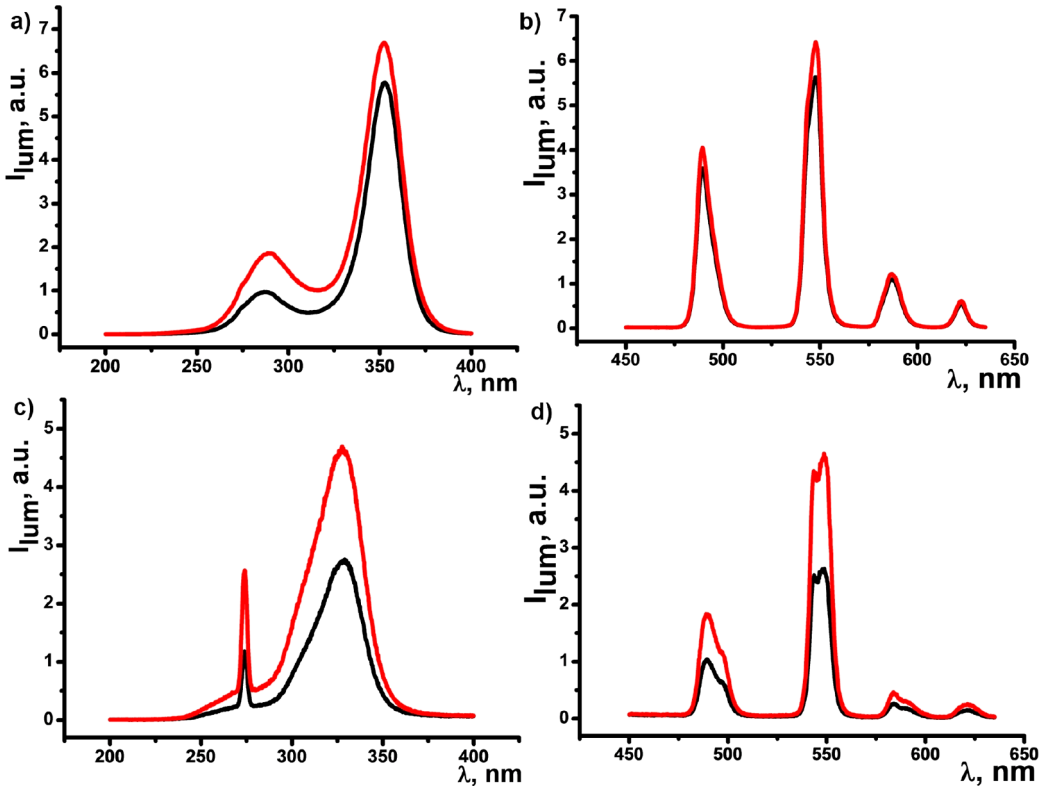

Figure 5. (a and c) Excitation and (b and d) emission spectra of PSS-[Tb_2(TCA2)$_2$] (a and b) and PSS-[TbCA1] (c and d) colloids in H_2O (black) and D_2O (red).

$A_{489} \cong 2.5$) reflect the different coordination modes of the lanthanide ions provided by TCA*i* and CA*i* ligands.

The values of the excited state lifetime evaluated from the luminescence decay curves (Figure S3) confirm the difference in the hydration number of the lanthanide ions in the complexes with TCA*i* and CA*i* ligands. In fact, using an A_{Tb} value of 4.2[39] and the lifetimes determined for colloids in H_2O and D_2O (Table 2), q values of 2.1 and 4.4 were obtained using eq 12 for PSS-[Tb_2(TCA2)$_2$] and PSS-[TbCA1], respectively.

Table 2. Excited State Lifetimes for PSS-[Tb_2(TCA2)$_2$] and PSS-[TbCA1] Colloids in H_2O (τ_{H_2O}) and D_2O (τ_{D_2O}) and Hydration Number Values (q)

	τ_{H_2O} (ms)	τ_{D_2O} (ms)	q
PSS-[Tb_2(TCA2)$_2$]	0.704 ± 0.001	1.087 ± 0.002	2.1
PSS-[TbCA1]	0.351 ± 0.001	0.556 ± 0.001	4.4

Paramagnetic Relaxation Enhancement of Water Protons in PSS-[Gd_2(TCA*i*)$_2$] and PSS-[GdCA*i*] Colloids. Relaxation enhancement of water protons in PSS-[Gd_2(TCA*i*)$_2$] and PSS-[GdCA*i*] colloids was evaluated at 20.8 MHz by determining the longitudinal (r_1) and transverse (r_2) relaxivity values. For this purpose, the corresponding relaxation rates, R_1 and R_2, were measured on samples containing different Gd concentrations, obtained by dilution of an original sample, and relaxivities were derived by fitting the linear dependence on concentration to eq 1 (Figure S6); r_1 and r_2 values are listed in Table 3. Calix[4]arene-based systems show r_i values higher than those of thiacalix[4]arene-based ones, PSS-[GdCA1] showing the highest values. Relaxivity values of PSS-[Gd_2(TCA*i*)$_2$] colloids are lower than those reported for the water soluble complex of Gd(III) with thiacalix[4]arene-*p*-tetrasulfonate.[40] Relaxivity values of PSS-[GdCA*i*] colloids are on the order of or higher than those reported at the same magnetic field for colloids based on Gd(III) complexes with calix[4]arene ligands bearing four 1,3-diketone groups in the upper rim.[17,19] Moreover, r_i values for TCA*i*- and CA*i*-based systems are lower and higher than those reported for Gd(III) molecular complexes, respectively.[12]

Table 3. Longitudinal (r_1) and Transverse (r_2) Relaxivity Values of Water Protons in PSS-[Gd_2(TCA*i*)$_2$] and PSS-[GdCA*i*] Colloids at 20.8 MHz and 25 °C

	r_1 (mM^{-1} s^{-1})	r_2 (mM^{-1} s^{-1})
PSS-[Gd_2(TCA1)$_2$]	2.6 ± 0.1	3.6 ± 0.1
PSS-[Gd_2(TCA2)$_2$]	2.5 ± 0.1	3.8 ± 0.1
PSS-[Gd_2(TCA3)$_2$]	1.8 ± 0.1	2.7 ± 0.1
PSS-[GdCA1]	20.8 ± 0.5	24.7 ± 0.5
PSS-[GdCA2]	7.7 ± 0.2	9.6 ± 0.2
PSS-[GdCA3]	14.4 ± 0.3	17.3 ± 0.2

To better understand the origin of the differences in relaxation enhancement in the investigated systems, ^{1}H FFC NMR experiments were performed between 0.01 and 35 MHz. Figure 6 shows the $R_{1,para}$ NMRD curves, obtained after subtraction of the diamagnetic contribution $R_{1,0}$ from the relaxation rate R_1. $R_{1,0}$ was determined as the intercept in the fitting of R_1 versus [Gd] with eq 1. The curves displayed a shape typical of Gd(III) complexes with slow rotational mobility.[14,29] In particular, for PSS-[Gd_2(TCA*i*)$_2$] samples, $R_{1,para}$ was almost constant in the low-frequency range between 0.01 and 0.8 MHz, while a dispersion occurred in the 0.8−4 MHz interval, and a broad peak appeared at higher frequencies,

https://dx.doi.org/10.1021/acs.jpcc.0c00312
J. Phys. Chem. C XXXX, XXX, XXX−XXX

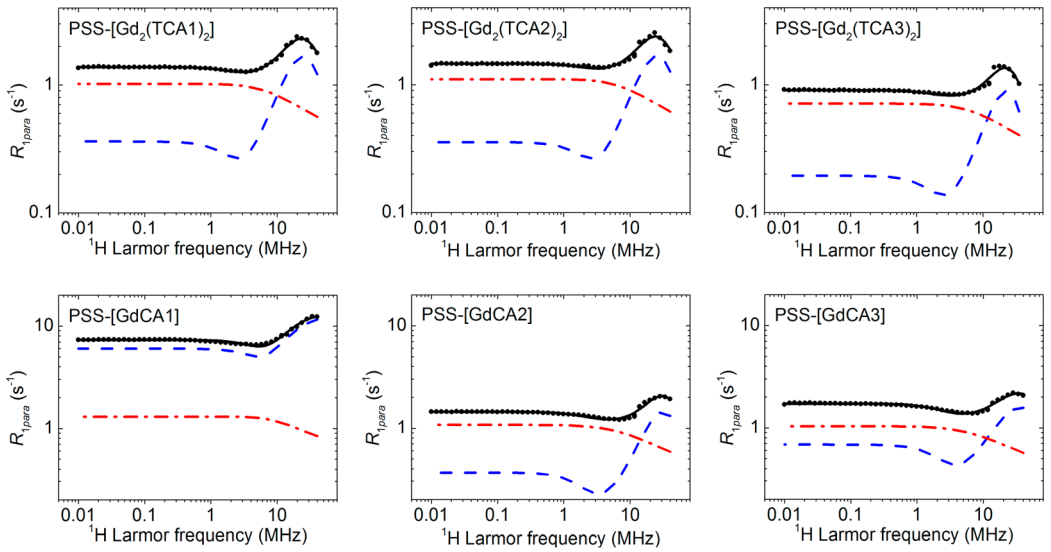

Figure 6. Experimental (dots) and representative fitting (black line) ^{1}H $R_{1,para}$ NMRD curves of water protons in colloids at 25 °C. Blue dashed and red dotted−dashed lines represent IS and OS contributions to $R_{1,para}$, respectively. The values of the best fitting parameters are listed in Table 4.

Table 4. Best Fit Parameters Obtained by Fitting the $R_{1,para}$ NMRD Curves of PSS-[Gd_2(TCA*i*)$_2$] and PSS-[GdCA*i*] Colloids

	$C_{M,ICP}$ (mM)	$C_{M,best}$ (mM)	q	τ_R (ns)	τ_m (ns)	τ_v (ps)	Δ^2 ($\times 10^{-19}$ s^{-2})
PSS-[Gd_2(TCA1)$_2$]	0.68 ± 0.03	0.16−0.20	0.1−0.3	≥5	50−300	42−48	1.1−1.6
PSS-[Gd_2(TCA2)$_2$]	0.64 ± 0.12	0.12−0.20	0.1−0.4	≥8	50−500	37−48	1.2−2.2
PSS-[Gd_2(TCA3)$_2$]	0.62 ± 0.08	0.10−0.13	0.07−0.20	≥3	10−300	45−49	1.0−1.5
PSS-[GdCA1]	0.29 ± 0.01	0.18−0.48	2.1−4.3	0.4−1	300−1100	24−26	4.8−6.0
PSS-[GdCA2]	0.27 ± 0.02	0.16−0.20	0.1−0.4	≥5	30−500	25−30	1.9−3.2
PSS-[GdCA3]	0.15 ± 0.01	0.16−0.20	0.3−0.8	≥5	500−900	21−23	2.9−3.7

Table 5. Best Fit Parameters Obtained by Fitting the $R_{1,para}$ NMRD Curves of PSS-[Gd_2(TCA*i*)$_2$] and PSS-[GdCA*i*] Colloids with q Fixed at the Value Expected from Gd(III) Coordination in the Complexes

	$C_{M,ICP}$ (mM)	$C_{M,best}$ (mM)	q	τ_R (ns)	τ_m (μs)	τ_v (ps)	Δ^2 ($\times 10^{-19}$ s^{-2})
PSS-[Gd_2(TCA1)$_2$]	0.68 ± 0.03	0.07	2	≥30	1.1	37	2.0
PSS-[Gd_2(TCA2)$_2$]	0.64 ± 0.12	0.08	2	≥30	1.3	35	2.4
PSS-[Gd_2(TCA3)$_2$]	0.62 ± 0.08	0.05	2	≥30	1.6	35	2.1
PSS-[GdCA1]	0.29 ± 0.01	0.29	4	0.4−1	0.3−1.1	25−26	4.8−5.6
PSS-[GdCA2]	0.27 ± 0.02	0.07	4	≥10	2.2	20	5.3
PSS-[GdCA3]	0.15 ± 0.01	0.07	4	≥10	2.4	18	4.8

with a maximum at ∼24 MHz. On the other hand, for PSS-[GdCA*i*] samples, the dispersion was observed between 0.6 and 5 MHz and the maximum occurred at ∼30 MHz for PSS-[GdCA2] and PSS-[GdCA3] and was at the limit of the investigated frequency region for PSS-[GdCA1]. The slow rotational mobility is most probably associated with the formation of nanoparticles constituted by self-assembled Gd complexes. To characterize the Gd(III) species responsible for the relaxation properties observed for the different samples, the $R_{1,para}$ curves were analyzed in terms of the PRE theory (see Theoretical Basis). Given the high number of unknown parameters and the correlations among them, the analysis was performed by fixing some of them on the basis of the literature.[2,41] In particular, the assumptions a_{GdH} = 3.1 Å and D_{GdH} = 2.3 × 10^{-9} m^2 s^{-1} (corresponding to the diffusion constant of water at 25 °C) were made for the R_1^{OS} contribution, while we fixed an r_{GdH} of 3.05 Å for the R_1^{IS} one. Very good fittings were obtained for all samples with parameters in the ranges listed in Table 4; representative fitting curves are shown in Figure 6, together with the R_1^{IS} and R_1^{OS} contributions.

For the PSS-[Gd_2(TCA*i*)$_2$] colloids, the best fit values of the Gd(III) concentration, $C_{M,best}$, were roughly 3−5 times smaller than $C_{M,ICP}$ and those of q were <0.4, much lower than the value expected on the basis of Gd(III) coordination in the complexes (q = 2). Moreover, the best fit value of τ_m was between 10 and 500 ns, whereas the correlation time for the reorientation of the Gd−H vector, τ_R, had a lower limit value of 3−8 ns. On the basis of the Stokes−Einstein relationship, τ_R can be used to estimate the diameter of the species to which the Gd−H vector is rigidly bonded. In our case, τ_R values corresponded to a minimum diameter of 2.9−4.0 nm. If the fittings were performed by fixing q = 2, acceptable reproductions fo data (Figure 6) were obtained with very small $C_{M,best}$ values, even less than one-tenth of $C_{M,ICP}$, τ_m = 1.1−1.6 μs, and τ_R ≥ 30 ns (Table 5), corresponding to a minimum diameter of 6.1 nm. These findings indicate that only a fraction of water molecules coordinated to Gd(III) have

https://dx.doi.org/10.1021/acs.jpcc.0c00312
J. Phys. Chem. C XXXX, XXX, XXX−XXX

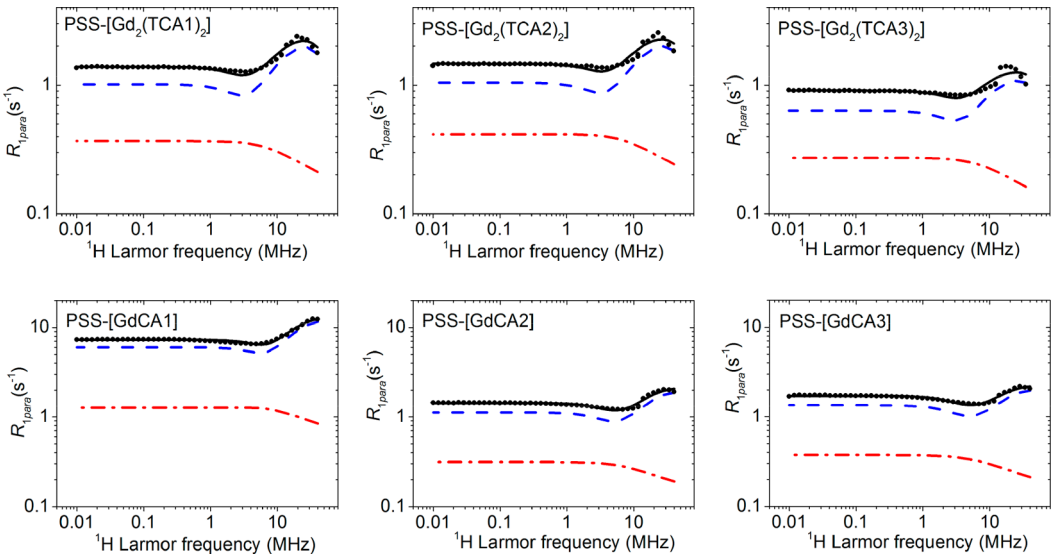

Figure 7. Experimental (dots) and best fitting (black line) ^{1}H $R_{1,para}$ NMRD curves of water protons in colloids at 25 °C. Blue dashed and red dotted−dashed lines represent IS and OS contributions to $R_{1,para}$, respectively. The calculated curves were obtained by fixing q = 2 for PSS-[Gd_2(TCAi)$_2$] colloids and q = 4 for PSS-[GdCAi] colloids and values of the remaining parameters listed in Table 5.

an exchange rate fast enough to contribute to relaxation enhancement and/or only a fraction of Gd(III) complexes are accessible to bulk water. The two situations correspond to quite different relative IS and OS contributions to relaxation enhancement. It must be noticed that an unexpectedly low relaxivity was also reported for a water soluble Gd(III) complex with thiacalix[4]arene-*p*-tetrasulfonate notwithstanding a q value of 2.4 and ascribed to an extremely slow exchange rate of coordinated water molecules associated with the very rigid coordination geometry of the complex.[40]

With regard to the PSS-[GdCAi] colloids, PSS-[GdCA1] was the only sample for which a good reproduction of the NMRD curves could be obtained with a range of best fit C_M values that included $C_{M,ICP}$ and q ranging from 2.1 to 4.3. Fixing $C_M = C_{M,ICP}$ and q = 4, the value determined by the Horrocks equation, we obtained very good fittings with τ_R = 0.4−1 ns, τ_m = 300−1100 ns, τ_v = 25−26 ps, and Δ^2 = 4.8−5.6 × 10^{19} s^{-2} (Table 5), as exemplified in Figure 7. Using the Stokes−Einstein relationship, from τ_R we can estimate a diameter of 1.5−2 nm for the species bearing the Gd−H vector. On the other hand, for PSS-[GdCA2] and PSS-[GdCA3], the best fit values of q were <1, much smaller than expected on the basis of Gd(III) coordination for CAi complexes, while $C_{M,best}$ was on the order of $C_{M,ICP}$ (Table 4). In particular, imposing $C_M = C_{M,ICP}$, very good data reproduction could be obtained with q = 0.1−0.2 for PSS-[GdCA2] and q = 0.7 for PSS-[GdCA3] and best fit values of the other parameters in the ranges reported in Table 4. In this case, a lower limit of 5 ns for PSS-[GdCA2] and PSS-[GdCA3] could be established for τ_R, corresponding to a minimum diameter of 3.4 nm. The found q values suggested that for PSS-[GdCA2] and PSS-[GdCA3] only a small fraction of coordinated H_2O molecules can be efficiently exchanged with the bulk, thus contributing to R_1^{IS}. As a result, for these samples, R_1^{IS} exceeds R_1^{OS} only in the frequency region where the maximum occurs, whereas $R_1^{IS} \gg R_1^{OS}$ for PSS-[GdCA1] over the entire frequency range (Figure 6). On the other hand, when the fitting was performed with q = 4 for PSS-[GdCA2] and PSS-[GdCA3], a comparably good data reproduction (Figure 7) was obtained with $C_{M,best} \ll C_{M,ICP}$, τ_m on the order of 2 μs, and $\tau_R \geq$ 10 ns (Table 5), corresponding to a minimum diameter of 4.3 nm. In this case, the main contribution to the relaxation rate arose from R_1^{IS} at all frequencies (Figure 7) and the lower relaxivity observed for PSS-[GdCA2] and PSS-[GdCA3] with respect to PSS-[GdCA1] could be mainly ascribed to the fact that Gd(III) is scarcely accessible to water.

CONCLUSIONS

Biocompatible hydrophilic colloids, potentially applicable as MRI positive contrast agents, were prepared for the first time by precipitation in an aqueous PSS solution of water insoluble Gd(III) complexes with TCAi and CAi ligands. The colloids, investigated by DLS and TEM, were found to be constituted by aggregates of nanoparticles, made by complexes, coated by PSS. Luminescence lifetime measurements on the Tb analogues allowed estimation of the mean hydration number q to be 2 and 4 per Gd(III) ion in the PSS-[Gd_2(TCAi)$_2$] and PSS-[GdCAi] colloids, respectively. Remarkably different relaxivity values at 20.8 MHz were found for the two classes of colloids, which could not be simply accounted for on the basis of q. Indeed, the analysis of ^{1}H NMRD curves in terms of PRE theory indicated that for the PSS-[GdCA1] colloid a quite high relaxivity results from q = 4 and a favorable combination of rotational motion of the Gd−H vectors in the nanoparticles and water exchange rate in the inner sphere. For the other PSS-[GdCAi] colloids, the relaxivity was limited by an extremely slow exchange rate for some of the water molecules in the inner sphere, manifested as q < 4 in the analysis of the NMRD curves, and/or by a scarce accessibility of bulk water to Gd(III) ions, as shown by best fit C_M values lower than those determined by ICP-OES. These two factors, which control IS and OS contributions, respectively, to relaxation enhancement of water protons, were found to be even more disadvantageous for the PSS-[Gd_2(TCAi)$_2$] colloids, for which relaxivity values were much lower than expected on the basis of the q value and the slow rotational motion of the nanoparticles. These findings could be ascribed to the rigid coordination geometry of Gd(III) in the sandwiched complexes with TCAi ligands,

https://dx.doi.org/10.1021/acs.jpcc.0c00312
J. Phys. Chem. C XXXX, XXX, XXX−XXX

which slows the water exchange kinetics, and to the larger size of nanoparticles, which partially hinders the accessibility of Gd(III) to water molecules.

■ ASSOCIATED CONTENT

Supporting Information

The Supporting Information is available free of charge at https://pubs.acs.org/doi/10.1021/acs.jpcc.0c00312.

UV−vis spectra of $[Tb_2(TCAi)_2]$ complexes and TCA*i* ligands in DMF and Jobs plots, cryo-TEM image of PSS-$[Tb_2(TCA2)_2]$ and corresponding nanoparticle size distribution diagram, luminescence decay curves of PSS-$[Tb_2(TCA2)_2]$ and PSS-[TbCA1] colloids in H_2O and D_2O, determination of Gd(III) and Tb(III) losses during colloid preparations, and longitudinal and transverse relaxation rates of water protons versus Gd concentration in PSS-$[Gd_2(TCAi)_2]$ and PSS-[GdCA*i*] colloids measured at a ^1H Larmor frequency of 20.8 MHz (PDF)

■ AUTHOR INFORMATION

Corresponding Author

Rustem Zairov − *Arbuzov Institute of Organic and Physical Chemistry, FRC Kazan Scientific Center, Russian Academy of Sciences, 420088 Kazan, Russian Federation; Kazan (Volga region) Federal University, 420008 Kazan, Russian Federation;* orcid.org/0000-0002-1699-6741; Phone: +7 843 2734573; Email: rustem02@yandex.ru; Fax: +7 843 2731872

Authors

Silvia Pizzanelli − *Istituto di Chimica dei Composti OrganoMetallici (ICCOM), Consiglio Nazionale delle Ricerche (CNR), 56124 Pisa, Italy*

Alexey P. Dovzhenko − *Kazan (Volga region) Federal University, 420008 Kazan, Russian Federation*

Irek Nizameev − *Kazan National Research Technical University named after A. N. Tupolev (KAI), 420111 Kazan, Russian Federation*

Anton Orekhov − *National Research Center "Kurchatov Institute", 123182 Moscow, Russia; Moscow Institute of Physics and Technology, 141700 Dolgoprudny, Moscow Region, Russia*

Natalya Arkharova − *A. V. Shubnikov Institute of Crystallography FSRC "Crystallography and Photonics" RAS, 119333 Moscow, Russia*

Sergey N. Podyachev − *Arbuzov Institute of Organic and Physical Chemistry, FRC Kazan Scientific Center, Russian Academy of Sciences, 420088 Kazan, Russian Federation*

Svetlana Sudakova − *Arbuzov Institute of Organic and Physical Chemistry, FRC Kazan Scientific Center, Russian Academy of Sciences, 420088 Kazan, Russian Federation*

Asiya R. Mustafina − *Arbuzov Institute of Organic and Physical Chemistry, FRC Kazan Scientific Center, Russian Academy of Sciences, 420088 Kazan, Russian Federation*

Lucia Calucci − *Istituto di Chimica dei Composti OrganoMetallici (ICCOM), Consiglio Nazionale delle Ricerche (CNR), 56124 Pisa, Italy;* orcid.org/0000-0002-3080-8807

Complete contact information is available at: https://pubs.acs.org/10.1021/acs.jpcc.0c00312

Notes

The authors declare no competing financial interest.

■ ACKNOWLEDGMENTS

The authors gratefully acknowledge the Assigned Spectral-Analytical Center of FRC Kazan Scientific Center of RAS. M. C. Mascherpa is thanked for performing ICP-OES analysis. M. Geppi is kindly acknowledged for letting us use the 20.8 MHz NMR spectrometer. This work was supported by the Ministry of Science and Higher Education within the State assignment FSRC "Crystallography and Photonics" RAS with respect to cryo-TEM images. PSS-stabilized colloids were prepared in KFU, and luminescence spectra were recorded in IOPC KSC RAS (R.Z.).

■ ABBREVIATIONS

FFC, fast field cycling; PRE, paramagnetic relaxation enhancement; NMRD, nuclear magnetic relaxation dispersion

■ REFERENCES

(1) Caravan, P. Strategies for Increasing the Sensitivity of Gadolinium Based MRI Contrast Agents. *Chem. Soc. Rev.* **2006**, *35*, 512−523.

(2) Botta, M.; Tei, L. Relaxivity Enhancement in Macromolecular and Nanosized Gd^{III}-Based MRI Contrast Agents. *Eur. J. Inorg. Chem.* **2012**, *2012*, 1945−1960.

(3) Hu, F.; Joshi, H. M.; Dravid, V. P.; Meade, T. J. High-Performance Nanostructured MR Contrast Probes. *Nanoscale* **2010**, *2*, 1884−1891.

(4) Huang, C.-H.; Tsourkas, A. Gd-Based Macromolecules and Nanoparticles as Magnetic Resonance Contrast Agents for Molecular Imaging. *Curr. Top. Med. Chem.* **2013**, *13*, 411−421.

(5) Zhang, L.; Liu, R.; Peng, H.; Li, P.; Xu, Z.; Whittaker, A. K. The Evolution of Gadolinium Based Contrast Agents: from Single-Modality to Multi-Modality. *Nanoscale* **2016**, *8*, 10491−10510.

(6) Yang, C.-T.; Padmanabhan, P.; Gulyás, B. Z. Gadolinium(III) Based Nanoparticles for T1-Weighted Magnetic Resonance Imaging Probes. *RSC Adv.* **2016**, *6*, 60945−60966.

(7) Padmanabhan, P.; Kumar, A.; Kumar, S.; Chaudhary, R. K.; Gulyás, B. Nanoparticles in Practice for Molecular-Imaging Applications: An Overview. *Acta Biomater.* **2016**, *41*, 1−16.

(8) Ni, D.; Bu, W.; Ehlerding, E. B.; Cai, W.; Shi, J. Engineering of Inorganic Nanoparticles as Magnetic Resonance Imaging Contrast Agents. *Chem. Soc. Rev.* **2017**, *46*, 7438−7468.

(9) Smith, B. R.; Gambhir, S. S. Nanomaterials for In Vivo Imaging. *Chem. Rev.* **2017**, *117*, 901−986.

(10) Wahsner, J.; Gale, E. M.; Rodríguez-Rodríguez, A.; Caravan, P. Chemistry of MRI Contrast Agents: Current Challenges and New Frontiers. *Chem. Rev.* **2019**, *119*, 957−1057.

(11) Li, H.; Meade, T. J. Molecular Magnetic Resonance Imaging with Gd(III)-Based Contrast Agents: Challenges and Key Advances. *J. Am. Chem. Soc.* **2019**, *141*, 17025−17041.

(12) Caravan, P.; Ellison, J. J.; McMurry, T. J.; Lauffer, R. B. Gadolinium(III) Chelates as MRI Contrast Agents: Structure, Dynamics and Applications. *Chem. Rev.* **1999**, *99*, 2293−2352.

(13) Caravan, P.; Farrar, C. T.; Frullano, L.; Uppal, R. Influence of Molecular Parameters and Increasing Magnetic Field Strength on Relaxivity of Gadolinium- and Manganese-Based T_1 Contrast Agents. *Contrast Media Mol. Imaging* **2009**, *4*, 89−100.

(14) Hermann, P.; Kotek, J.; Kubíček, V.; Lukeš, I. Gadolinium (III) Complexes as MRI Contrast Agents: Ligand Design and Properties of the Complexes. *Dalton Trans* **2008**, 3027−3047.

(15) Rieter, W. J.; Taylor, K. M. L.; An, H.; Lin, W.; Lin, W. Nanoscale Metal-Organic Frameworks as Potential Multimodal Contrast Enhancing Agents. *J. Am. Chem. Soc.* **2006**, *128*, 9024−9025.

(16) Perrier, M.; Kenouche, S.; Long, J.; Thangavel, K.; Larionova, J.; Goze-Bac, C.; Lascialfari, A.; Mariani, M.; Baril, N.; Guérin, C.;

et al. Investigation on NMR Relaxivity of Nano-Sized Cyano-Bridged Coordination Polymers. *Inorg. Chem.* **2013**, *52*, 13402−13414.
(17) Shamsutdinova, N. A.; Gubaidullin, A. T.; Odintsov, B. M.; Larsen, R. J.; Schepkin, V. D.; Nizameev, I. R.; Amirov, R. R.; Zairov, R. R.; Sudakova, S. N.; Podyachev, S. N.; et al. Polyelectrolyte-Stabilized Nanotemplates Based on Gd(III) Complexes with Macrocyclic Tetra-1,3-Diketones as a Positive MR Contrast Agents. *ChemistrySelect* **2016**, *1*, 1377−1383.
(18) Zairov, R.; Mustafina, A.; Shamsutdinova, N.; Nizameev, I.; Moreira, B.; Sudakova, S.; Podyachev, S.; Fattakhova, A.; Safina, G.; Lundstrom, I.; et al. High Performance Magneto-Fluorescent Nanoparticles Assembled from Terbium and Gadolinium 1,3-Diketones. *Sci. Rep.* **2017**, *7*, 40486.
(19) Zairov, R.; Khakimullina, G.; Podyachev, S.; Nizameev, I.; Safiullin, G.; Amirov, R.; Vomiero, A.; Mustafina, A. Hydration Number: Crucial Role in Nuclear Magnetic Relaxivity of Gd(III) Chelate-Based Nanoparticles. *Sci. Rep.* **2017**, *7*, 14010.
(20) Shamsutdinova, N.; Zairov, R.; Nizameev, I.; Gubaidullin, A.; Mukhametshina, A.; Podyachev, S.; Ismayev, I.; Kadirov, M.; Voloshina, A.; Mukhametzyanov, T.; et al. Tuning Magnetic Relaxation Properties of "Hard-Cores" in Core-Shell Colloids by Modification of "Soft Shell. *Colloids Surf., B* **2018**, *162*, 52−59.
(21) Zairov, R.; Shamsutdinova, N.; Podyachev, S.; Sudakova, S.; Gimazetdinova, G.; Rizvanov, I.; Syakaev, V.; Babaev, V.; Amirov, R.; Mustafina, A. Structure Impact in Antenna Effect of Novel Upper Rim Substituted Tetra-1,3-diketone Calix[4]arenes on Tb(III) Green and Yb(III) NIR-Luminescence. *Tetrahedron* **2016**, *72*, 2447−2455.
(22) Podyachev, S. N.; Sudakova, S. N.; Nagimov, R. N.; Lapaev, D. V.; Masliy, A. N.; Syakaev, V. V.; Bazanova, O. B.; Gimazetdinova, G. Sh.; Babaev, V. M.; Kuznetsov, A. M.; et al. Structural and Photophysical Properties of Tb^{3+}-Tetra-1,3-diketonate Complexes Controlled by Tetrathiacalix[4]arene Scaffolds. *Dalton Trans* **2019**, *48*, 3930−3940.
(23) Podyachev, S. N.; Sudakova, S. N.; Gimazetdinova, G. Sh.; Shamsutdinova, N. A.; Syakaev, V. V.; Barsukova, T. A.; Iki, N.; Lapaev, D. V.; Mustafina, A. R. Synthesis, Metal Binding and Spectral Properties of Novel bis-1,3-Diketone Calix[4]arenes. *New J. Chem.* **2017**, *41*, 1526−1537.
(24) Podyachev, S. N.; Gimazetdinova, G. Sh.; Sudakova, S. N.; Shamsutdinova, N. A.; Lapaev, D. V.; Syakaev, V. V.; Gubaidullin, A. T.; Nagimov, R. N.; Mustafina, A. R. Influence of Upper Rim Dibromo-Substitution in bis-1,3-Diketone Calix[4]arenes on Spectral Properties of Ligands and Their Lanthanide Complexes. *Tetrahedron* **2017**, *73*, 5397−5407.
(25) Horrocks, W. D.; Sudnick, D. R. Lanthanide Ion Probes of Structure in Biology. Laser-Induced Luminescence Decay Constants Provide a Direct Mesaure of the Number of Metal-Coordinated Water Molecules. *J. Am. Chem. Soc.* **1979**, *101*, 334−340.
(26) Horrocks, W. D.; Sudnick, D. R. Lanthanide Ion Luminescence Probes of the Structure of Biological Macromolecules. *Acc. Chem. Res.* **1981**, *14*, 384−392.
(27) Anoardo, E.; Galli, G.; Ferrante, G. Fast-Field-Cycling NMR: Applications and Instrumentation. *Appl. Magn. Reson.* **2001**, *20*, 365−404.
(28) Kimmich, R.; Anoardo, E. Field-Cycling NMR Relaxometry. *Prog. Nucl. Magn. Reson. Spectrosc.* **2004**, *44*, 257−320.
(29) Aime, S.; Botta, M.; Esteban-Gómez, D.; Platas-Iglesias, C. Characterisation of Magnetic Resonance Imaging (MRI) Contrast Agents Using NMR Relaxometry. *Mol. Phys.* **2019**, *117*, 898−909.
(30) Kumagai, H.; Hasegawa, M.; Miyanari, S.; Sugawa, Y.; Sato, Y.; Hori, T.; Ueda, S.; Kamiyama, H.; Miyano, S. Facile Synthesis of *p-tert*-Butylthiacalix[4]arene by the Reaction of *p-tert*-Butylphenol with Elemental Sulfur in the Presence of a Base. *Tetrahedron Lett.* **1997**, *38*, 3971−3972.
(31) Higuchi, Y.; Narita, M.; Niimi, T.; Ogawa, N.; Hamada, F.; Kumagai, H.; Iki, N.; Miyano, S.; Kabutod, C. Fluorescent Chemo-Sensor for Metal Cations Based on Thiacalix[4]arenes Modified with Dansyl Moieties at the Lower Rim. *Tetrahedron* **2000**, *56*, 4659−4666.
(32) Bertini, I.; Luchinat, C.; Parigi, G.; Ravera, E. *NMR of Paramagnetic Molecules. Applications to Metallobiomolecules and Models*, 2nd ed.; Elsevier: Amsterdam, 2017.
(33) Solomon, I. Relaxation Processes in a System of Two Spins. *Phys. Rev.* **1955**, *99*, 559−565.
(34) Bloembergen, N.; Morgan, L. O. Proton Relaxation Times in Paramagnetic Solutions. Effects of Electron Spin relaxation. *J. Chem. Phys.* **1961**, *34*, 842−850.
(35) Belorizky, E.; Fries, P. H. Simple Analytical Approximation of the Longitudinal Electronic Relaxation Rate of Gd(III) Complexes in Solutions. *Phys. Chem. Chem. Phys.* **2004**, *6*, 2341−2351.
(36) Freed, J. H. Dynamic Effects of Pair Correlation Functions on Spin Relaxation by Translational Diffusion in Liquids. II. Finite Jumps and Independent T_1 Processes. *J. Chem. Phys.* **1978**, *68*, 4034−4037.
(37) Hwang, L.-P.; Freed, J. H. Dynamic Effect of Pair Correlation Functions on Spin Relaxation by Translational Diffusion in Liquids. *J. Chem. Phys.* **1975**, *63*, 4017−4025.
(38) Barge, A.; Cravotto, G.; Gianolio, E.; Fedeli, F. How to Determine Free Gd and Free Ligand in Solution of Gd Chelates. A Technical Note. *Contrast Media Mol. Imaging* **2006**, *1*, 184−188.
(39) Bünzli, J.-C. G. Lanthanide Luminescence for Biomedical Analyses and Imaging. *Chem. Rev.* **2010**, *110*, 2729−2755.
(40) Iki, N.; Boros, E.; Nakamura, M.; Baba, R.; Caravan, P. Gd_3TCAS_2: An Aquated Gd^{3+}-Thiacalix[4]arene Sandwich Cluster with Extremely Slow Ligand Substitution Kinetics. *Inorg. Chem.* **2016**, *55*, 4000−4005.
(41) Holz, M.; Heil, S. R.; Sacco, A. Temperature-Dependent Self-Diffusion Coefficients of Water and Six Selected Molecular Liquids for Calibration in Accurate ^{1}H NMR PFG Measurements. *Phys. Chem. Chem. Phys.* **2000**, *2*, 4740−4742.

https://dx.doi.org/10.1021/acs.jpcc.0c00312
J. Phys. Chem. C XXXX, XXX, XXX−XXX